ELSEVIER

Chemical Engineering Journal 135S (2008) S179–S184

Chemical Engineering Journal

www.elsevier.com/locate/cej

Testing and simulation of ceramic micro heat exchangers

B. Alm [a,*], U. Imke [b], R. Knitter [a], U. Schygulla [c], S. Zimmermann [c]

[a] *Institut für Materialforschung III (IMF III), Forschungszentrum Karlsruhe GmbH, P.O. Box 3640, 76021 Karlsruhe, Germany*
[b] *Institut für Reaktorsicherheit (IRS), Forschungszentrum Karlsruhe GmbH, P.O. Box 3640, 76021 Karlsruhe, Germany*
[c] *Institut für Mikroverfahrenstechnik (IMVT), Forschungszentrum Karlsruhe GmbH, P.O. Box 3640, 76021 Karlsruhe, Germany*

Abstract

Ceramic microstructure devices in form of counterflow and crossflow microchannel heat exchangers have been manufactured to be used in thermal and chemical process engineering. The performance has been tested using water as a test fluid with maximum flow rates of 120 kg/h. The results of the measurements are compared with global estimations using standard correlations for heat exchangers and a more detailed simulation using a local porous body approach of the micro structured region. The devices show stronger heat transfer and pressure loss than predicted by theoretical considerations. This result is mainly explained by effects of channel blockages arising from the joining process.

Keywords: Ceramic; Heat exchanger; Simulation

1. Introduction

Ceramic micro structured components open up new fields of application in micro process engineering, e.g. for high-temperature reactions or reactions with corrosive media, for which polymer or metal components are not suitable [1–3]. However, the fabrication of ceramic components is more difficult and the minimum size of the walls between the microchannels is limited due to mechanical stability reasons and fabrication constraints. A large rate of heat transfer based on the large heat transfer area to volume ratio is a unique feature of micro heat exchangers [4].

It is necessary to test the heat transfer performance of a typical device before applications. In addition it is advisable to evaluate the behavior of a microchannel heat exchanger by some simulation tool to avoid expensive measurements. In the present paper a numerical approach based on empirical models and realized in the TwoPorFlow code is used to simulate microchannel heat exchangers. This has several advantages compared to the use of more sophisticated geometry resolving up to date commercial CFD tools. Complete simulations of complex heat exchanger geometries require large computer resources using many elementary volumes to resolve the fluid channels and the heat transferring structure. The simplified tool models the main physical processes like heat conduction inside the solid structure, heat transfer to the fluid and pressure loss by known empirical correlations. This makes the calculation more efficient and flexible. Characteristic data depending on different boundary and operating conditions can be produced using coarse meshing compared to usual CFD applications. Different channel geometries can be introduced simply by the hydraulic diameter combined with appropriate correlations for the Nusselt number. Switching from laminar to turbulent flow conditions is automatically taken into account by the constitutive correlations.

2. Experimental procedure

Three different manufactured ceramic micro heat exchangers were applied as prototypes to check their performance at a system pressure of 8 bar. The alumina microcomponents were produced by a rapid prototyping process chain and subsequently assembled.

2.1. Manufacturing of ceramic micro heat exchangers

Based on a rapid prototyping process chain [5] ceramic microcomponents were produced by combining stereolithography and low-pressure injection molding (LPIM). LPIM is a suitable method for near net shape manufacturing of ceramic microcomponents. The sintered heat exchanger components were joined using a glass solder. The advantage of this joining method is based on the fact that individual channel plates may be finished to ensure coplanarity

* Corresponding author. Tel.: +49 7247 82 6100; fax: +49 7247 82 4612.
E-mail address: birgit.loebbecke@imf.fzk.de (B. Alm).

1385-8947/$ – see front matter © 2007 Elsevier B.V. All rights reserved.
doi:10.1016/j.cej.2007.07.005

Table 1
Geometry of two counterflow and one crossflow heat exchangers

Micro heat exchanger	Counterflow 1		Counterflow 2		Crossflow	
	Passage 1, cold water[a]	Passage 2, warm water[a]	Passage 1, cold water[a]	Passage 2, warm water[a]	Passage 1, cold water[a]	Passage 2, warm water[a]
Number of plates	3	3	2	2	2	2
Number of channels	17	17	17	17	17	17
Total number of channels	51	51	34	34	34	34
Channel length (mm)	12.5	12.5	12.5	12.5	12.5	12.5
Channel width (μm)	250	250	250	250	250	250
Channel height (μm)	420	320	420	340	380	335
Wall thickness (μm)	520	520	520	520	520	520
Layer thickness (μm)	880	990	895	965	690	940

[a] Medium.

in the heat exchanger system. The development, manufacturing, and first results of the ceramic 'counterflow 2' micro heat exchanger (see Table 1) have been described in [6].

The alumina heat exchangers were built in the counterflow and crossflow mode. A counterflow micro heat exchanger with two plates per passage is represented schematically in Fig. 1, on the top left. Below the principle setup two different channel plates for the cold and warm passage are shown. They were arranged in a laterally reversed manner in the assembled counterflow heat exchanger pictured in Fig. 1, on the right. The channel plates contain 17 microchannels. These channels have a width of 250 μm and a height ranging from 320 to 420 μm depending on the heat exchanger type. The wall between the channels is 520 μm thick. The separating layer between the passages is in the range of 690–990 μm. All channels have a length of 12.5 mm. The heat exchanger named 'counterflow 1' was setup with three channel plates per passage, 'counterflow 2' with two plates, and the 'crossflow' heat exchanger with two plates. In Table 1 the geometries used for both passages of the heat exchangers in counterflow and crossflow mode are summarized.

2.2. Measurement setup

The three ceramic micro heat exchangers were installed on a specially designed test rig and applied for cooling warm water at a system pressure of 8 bar. The alumina tubelets were fixed to the screws of the test rig using Teflon hose and Swagelok screw adapters. The ceramic heat exchangers 'counterflow 1' and 'crossflow' were measured with and without insulation (ceramic fiber mat, glass wool) and 'counterflow 2' without insulation, only. Fully demineralized water was used as working fluid. The nearly equal mass flow rates in both passages were increased in steps of 10 kg/h to maxima between 80 and 120 kg/h. For each step the mass flow rates, pressures, and temperatures at inlet and outlet were measured. The data were stored and converted into the corresponding physical parameters and characteristic numbers by a special evaluation program.

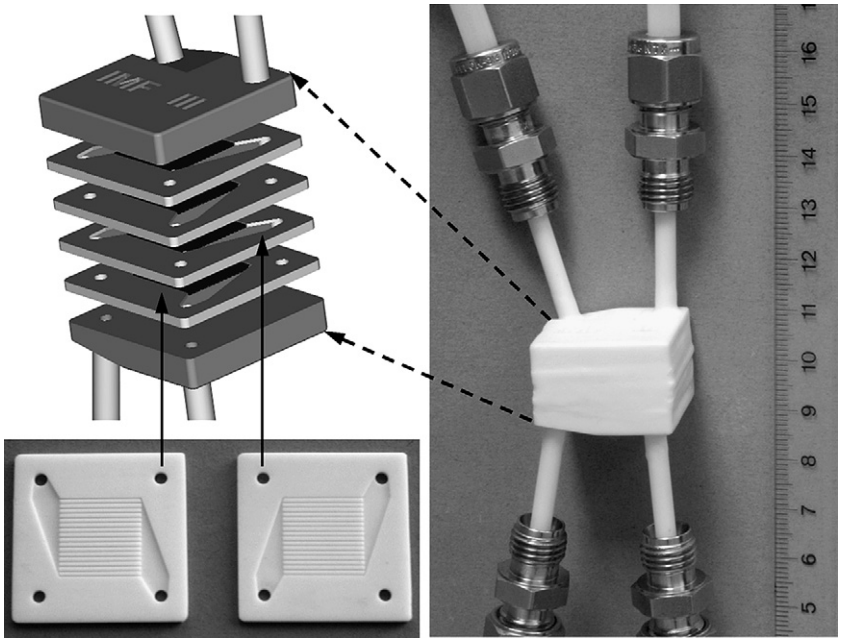

Fig. 1. Principle setup of a counterflow micro heat exchanger with two plates per passage, channel plates and a ceramic micro heat exchanger with media ports.

Table 2
Results of two counterflow and one crossflow heat exchangers

Counterflow 1 (insulated)											
$\dot{m}_{\text{Pass 1}}$ (kg/h)	20.4	30.5	40.8	50.5	60.4	70.6	81.4	90.4	99.8	109.9	120.3
$\dot{m}_{\text{Pass 2}}$ (kg/h)	21.0	29.8	40.0	50.1	60.7	70.7	81.3	90.9	100.2	109.7	120.8
ε	0.22	0.18	0.17	0.14	0.14	0.13	0.12	0.12	0.11	0.11	0.10
k_{exp} (kW/m^2 K)	8.7	10.5	12.2	13.4	14.6	15.6	16.7	17.4	18.3	19.0	19.5
Counterflow 2 (non-insulated)											
$\dot{m}_{\text{Pass 1}}$ (kg/h)	12.6	20.5	30.0	40.7	50.5	59.9	70.6	80.6			
$\dot{m}_{\text{Pass 2}}$ (kg/h)	12.4	20.9	32.5	41.2	53.5	60.6	70.4	78.8			
ε	0.19	0.16	0.13	0.11	0.09	0.08	0.08	0.07			
k_{exp} (kW/m^2 K)	7.0	8.7	10.3	11.6	12.6	13.4	14.3	15.0			
Crossflow (insulated)											
$\dot{m}_{\text{Pass 1}}$ (kg/h)	10.4	19.9	30.2	40.1	50.5	60.3	70.3	80.6	90.6	97.3	
$\dot{m}_{\text{Pass 2}}$ (kg/h)	10.5	20.6	30.0	40.6	50.8	60.4	70.9	80.2	91.0	98.0	
ε	0.22	0.18	0.15	0.14	0.13	0.13	0.12	0.11	0.11	0.10	
k_{exp} (kW/m^2 K)	7.0	10.1	12.4	14.4	16.6	18.2	19.7	21.1	22.2	22.2	

3. Comparison of experimental results and simulations

3.1. Measurement results and simple estimations

In order to calculate the heat transfer efficiency, the heat exchanger efficiency ε is used which relates the effectively transmitted heat quantity $\dot{Q}$ to the maximum transmissible heat quantity $\dot{Q}_{\max}$ [7]:

$$\dot{Q} = \dot{m}_{\text{c}} c_{pc} (T_{\text{ci}} - T_{\text{co}}) = \dot{m}_{\text{w}} c_{pw} (T_{\text{wo}} - T_{\text{wi}}) \quad (1)$$

$$\dot{Q}_{\max} = \min(\dot{m}_{\text{c}} c_{pc}; \dot{m}_{\text{w}} c_{pw})(T_{\text{ci}} - T_{\text{wi}}) \quad (2)$$

$$\varepsilon = \frac{\dot{Q}}{\dot{Q}_{\max}} = \frac{\dot{m}_{\text{c}} c_{pc} (T_{\text{ci}} - T_{\text{co}})}{\min(\dot{m}_{\text{c}} c_{pc}; \dot{m}_{\text{w}} c_{pw})(T_{\text{ci}} - T_{\text{wi}})} \quad (3)$$

$\dot{m}$ is the mass flow rate (c: cold; w: warm), c_p is the specific heat capacity and T_{ci}, T_{co}, T_{wi} and T_{wo} are the inlet and outlet temperatures of the cold and warm fluid, respectively.

For a constant product $\dot{m}$ c_p Eq. (3) can be simplified to a temperature difference ratio:

$$\varepsilon = \left(\frac{T_{\text{ci}} - T_{\text{co}}}{T_{\text{ci}} - T_{\text{wi}}} \right) = \left(\frac{T_{\text{wo}} - T_{\text{wi}}}{T_{\text{ci}} - T_{\text{wi}}} \right) \quad (4)$$

Concerning both investigations with and without insulation no significant difference was observed for the characteristics of type ‘counterflow 1’ and type ‘crossflow’ heat exchangers. Related to the heat transfer efficiency the influence of the insulation is small.

For water mass flow rates of 20 kg/h a heat transfer efficiency was reached for ‘counterflow 2’ of 0.16, for ‘crossflow’ of 0.18, and for ‘counterflow 1’ of 0.22, respectively. The maximum efficiency determined theoretically using Eq. (4) under the given test conditions amounts to 0.19. For this estimation, the measured inlet temperatures of both flow mediums are used, and only a single microchannel without the influence of boundary effects like media supply, outlet or mass flow inlet in the micro heat exchanger is considered. Consequently, the theoretical efficiencies have lower values than the experimentally determined efficiencies. Using increased mass flow rates of 30 kg/h the efficiencies decrease to the range of 0.13–0.18. For 120 kg/h a value of 0.10 was calculated. For all calculations a thermal conductivity of 25 W/m K was assumed. In Table 2 the experimental results of the efficiency and the heat transfer coefficient are summarized.

The behavior of the overall heat transfer coefficient in the tested counterflow and crossflow ceramic heat exchangers is shown in Fig. 2 compared with an estimated heat transfer coefficient. The experimental heat transfer coefficient k_{exp} is calculated by:

$$k_{\text{exp}} = \frac{\dot{Q}}{A \vartheta_{\text{m}}} \quad (5)$$

where A is the effective heat transfer surface, and ϑ_{m} is the logarithmic mean temperature.

The theoretically determined heat transfer coefficient k_{theor} is calculated from the heat transfer coefficients, α_{c} and α_{w}, at the cold and warm side:

$$\frac{1}{k_{\text{theor}}} = \frac{1}{\alpha_{\text{c}}} + \frac{1}{\alpha_{\text{w}}} + \frac{s}{\lambda} \quad (6)$$

where s is the thickness of the plate between both passages and λ denotes the thermal conductivity of alumina.

The heat transfer coefficients α are dependent on the Nusselt number, the thermal conductivity of water, and the microchannel

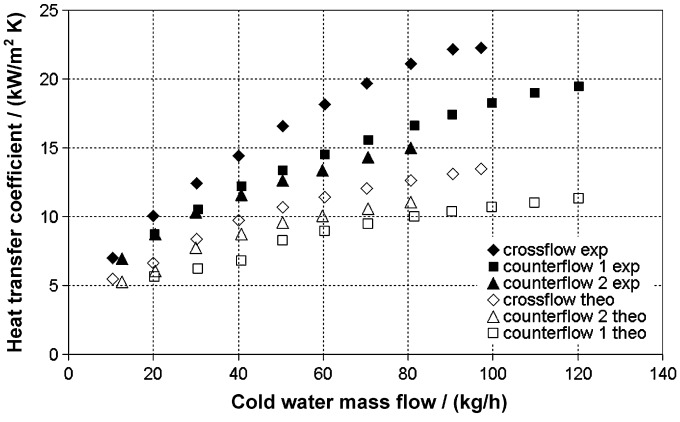

Fig. 2. Behavior of the heat transfer coefficient in ceramic micro heat exchangers.

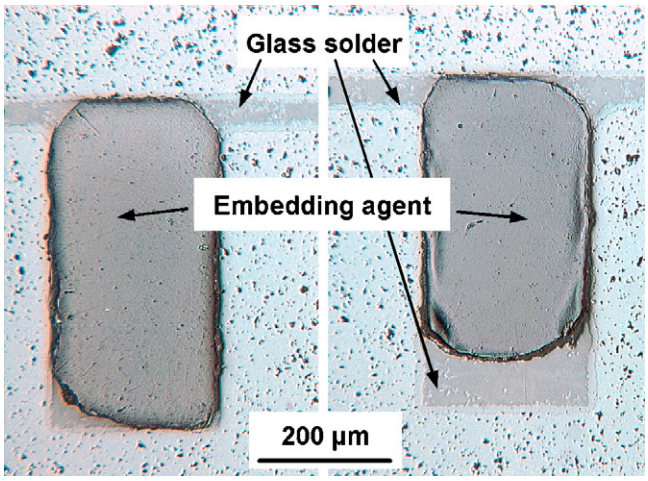

Fig. 3. Cross-sections of channel plates joined by soldering.

hydraulic diameter d_h [8]:

$$\alpha = \frac{Nu\ \lambda_{fluid}}{d_h} \tag{7}$$

The experimentally determined heat transfer coefficient k_{exp} according to Eq. (5) ranges from 7 to 22 kW/m^2 K, and is always higher than the theoretically calculated values. The highest measured values for the overall heat transfer coefficient were achieved with the crossflow heat exchanger, while the lowest values with 'counterflow 2'. The theoretical heat transfer coefficient ranges from 5 to 14 kW/m^2 K (see Fig. 2).

This deviation in heat transfer coefficients is attributed to the setup of the heat exchangers. During ceramization the glass solder occasionally enters the channels of the joined micro heat exchangers. As a consequence, there are some channels with reduced channel heights or even channels that are completely filled with glass solder in the tested micro heat exchangers (see Fig. 3). For the two counterflow heat exchangers the curves for theoretically and experimentally determined heat transfer coefficients are in reversed order. The hydraulic diameter seems to be stronger reduced in 'counterflow 1' than in 'counterflow 2', so that k_{exp} of 'counterflow 1' is larger than in 'counterflow 2'.

3.2. The TwoPorFlow code

To realize a simplified efficient simulation method taking into account the essential physical processes of flow and heat transfer in a microchannel heat exchanger a porous media approach is used. The code TwoPorFlow has been developed at the Forschungszentrum Karlsruhe to simulate single- and two-phase flow including heat transfer and phase change in multi-microchannel devices. The two-fluid model is taken to describe the flow of the liquid and gaseous fluids inside the one-dimensional channels. A detailed description of the basic equations and the numerical solution algorithm is given in [9]. In the present case the vapor volume fraction is set to zero and only the equations for the liquid component are solved. The solid structure is represented as a porous medium with its own temperature field. Wall friction and heat transfer between structure and fluid are modelled by conventional empirical correlations [8]. To solve the conservation equations for energy, mass and momentum in 3D Cartesian coordinates a semi-implicit numerical procedure based on the Implicit Continuous Eulerian (ICE) method is used. The coupling with the solid structure heat conduction calculation is done in an explicit manner. Steady states are calculated by a transient approach. It has been shown that the code gives reliable results in the application to metallic microchannel compact heat exchangers of counterflow and crossflow type [9].

3.3. Numerical simulation with TwoPorFlow

The application of the code is restricted to the micro structured core of the insulated heat exchangers, which have better thermal boundary conditions than the non-insulated ones. Due to the symmetry of the geometry it is adequate to consider one pair of microplates for cold and warm inlet flow. Fig. 4 shows the coarse Cartesian grid used for the two plates and the direction of flow in the case of counterflow. The stack of the two plates is substituted by a porous body with different volume porosities in the cold and the warm passage and subdivided into a mesh of 12 × 10 × 2 cells. The nearly triangular flat inlet and outlet regions are mapped by linear varying porosities and corresponding hydraulic diameters and heat exchange area con-

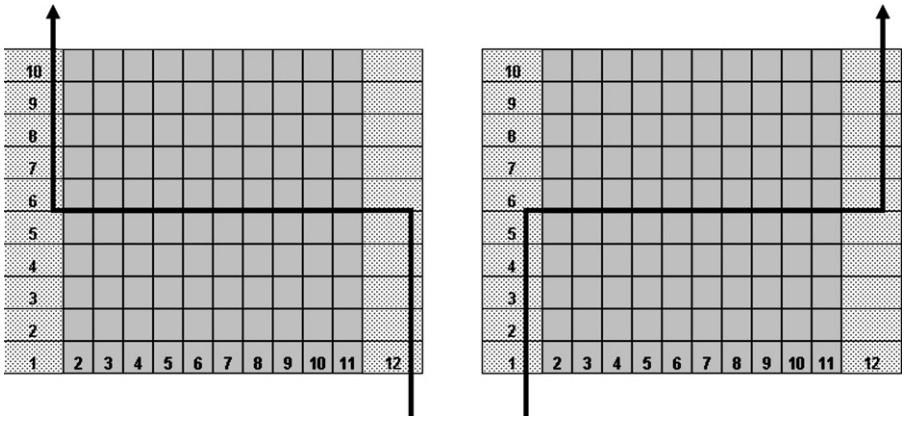

Fig. 4. TwoPorFlow mesh for counterflow heat exchanger.

centrations. Typical values in the straight channel region are 0.1 for the volume porosity, 0.3 mm for the hydraulic diameter and 1300 m^{-1} for the heat transfer area density. The convective part of the momentum equation is small compared to the friction source term created by the small sized channels, so the momentum convection is neglected and 90° flow direction changes are approximated by pressure loss coefficients equal to 1. The meshing of the crossflow heat exchanger is similar to Fig. 4, but one plate is rotated by 90°. Blocking walls which set the mass flow rate between the numerical cells to zero are used to force the flow directions and to separate the different passages, which are thermally coupled by the alumina structure with a thermal conductivity of 25 W/m K. The outlet pressure is given by the experimental settings. The mass flow rates of the initially cold water in one passage and the warm water in the other passage are taken from the measurements just as inlet and outlet water temperatures. The program calculates temperature changes and pressure losses along the core of the heat exchangers. In addition, local thermo-hydraulic conditions can be determined. For example Fig. 5 shows the water temperature distribution in the cold passage of the counterflow heat exchanger using a flow rate of about 20 kg/h. All temperatures are calculated in the mesh cell centers.

In Figs. 6–9 the simulated results for integral pressure loss and outlet temperatures are compared to the measured data. For the pressure loss the results underestimates clearly the experimental data, which are taken for the whole apparatus including the small alumina tubes and the connections to the teflon hoses. One part of the pressure loss takes place outside the heat exchanger core in the supplying pipes. For the maximum flow rate of 120 kg/h TwoPorFlow was used in a one dimensional approach to calculate the total pressure loss in the pipes with the result of about 0.9 bar.

Outlet

25.1	25.0	24.2	23.3	22.5	21.7	20.9	20.1	19.3	18.5	17.6	16.2
24.9	24.2	23.4	22.6	21.7	20.9	20.1	19.2	18.4	17.6	16.7	15.3
24.7	23.7	22.9	22.0	21.1	20.3	19.5	18.6	17.8	16.9	16.0	14.7
24.5	23.4	22.5	21.6	20.7	19.9	19.0	18.2	17.3	16.4	15.5	14.2
24.4	23.1	22.1	21.3	20.4	19.5	18.6	17.8	16.9	16.0	15.1	13.8
24.2	22.8	21.9	20.9	20.1	19.2	18.3	17.4	16.6	15.7	14.7	13.4
24.1	22.6	21.7	20.7	19.8	18.9	18.0	17.1	16.3	15.4	14.4	13.1
23.9	22.5	21.5	20.5	19.6	18.7	17.8	16.9	16.0	15.1	14.1	12.9
23.7	22.4	21.3	20.4	19.4	18.5	17.6	16.7	15.8	14.9	13.9	12.7
23.5	22.4	21.3	20.3	19.4	18.4	17.5	16.6	15.7	14.7	13.7	12.5

Inlet

Fig. 5. Simulated water temperature (°C) distribution in the cold 'counterflow 1' passage.

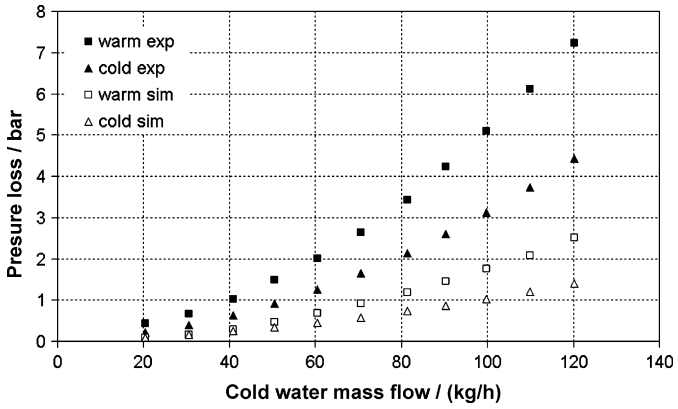

Fig. 6. Simulated and measured pressure loss in the 'counterflow 1' heat exchanger with insulation.

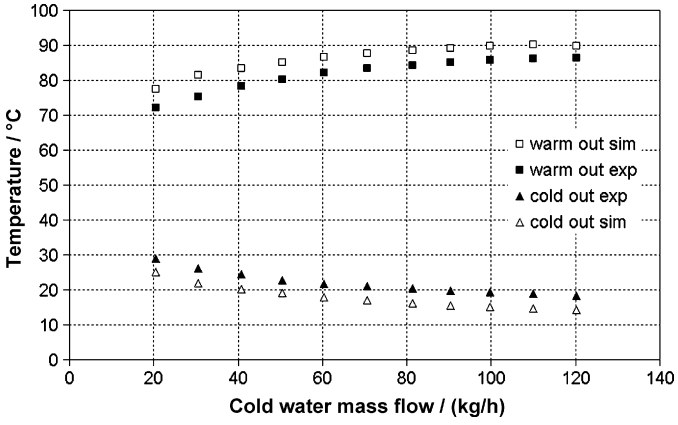

Fig. 7. Simulated and measured outlet temperatures in the 'counterflow 1' heat exchanger with insulation.

As mentioned in Section 3.1 for the heat transfer coefficient it was found that joining material could penetrate into the microchannels causing increased pressure loss by flow restrictions. The hydraulic diameter is strongly reduced at such locations leading to a stronger pressure loss coefficient.

In the case of the counterflow heat exchanger the pressure loss along the warm passage is stronger than along the cold passage (see Fig. 6) for the experimental data and the simulation although

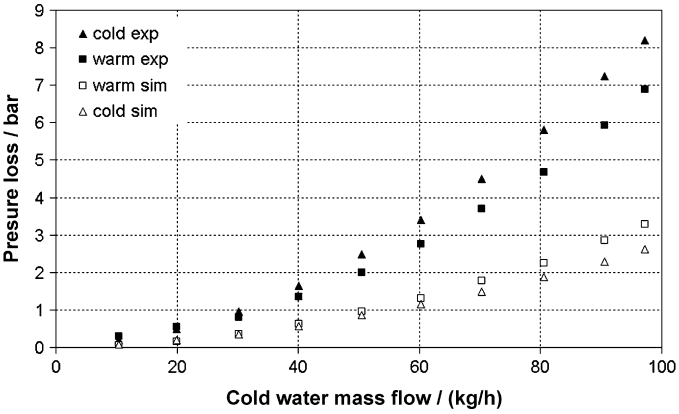

Fig. 8. Simulated and measured pressure loss in the 'crossflow' heat exchanger with insulation.

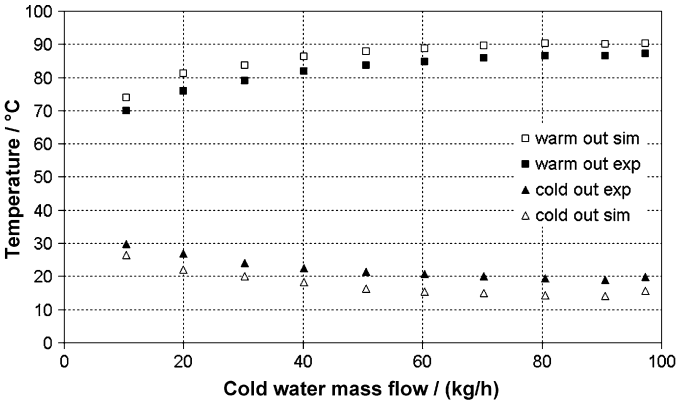

Fig. 9. Simulated and measured outlet temperatures in the 'crossflow' heat exchanger with insulation.

warm water has a lower viscosity than cold water leading to a smaller pressure loss for equal channel geometry. However, for the present case the channel height of the warm water passage is reduced by 100 μm compared to the channel height in the cold region (see Table 1). For the crossflow heat exchanger the difference is 45 μm, only. The difference in pressure loss between the two passages becomes smaller in the simulation (see Fig. 8). For the measured data we see, that the pressure loss in the cold region is larger than in the warm region, which could be attributed to a more pronounced blockage effect in this case.

The simulated outlet temperatures of warm and cold passages depending on the flow rate represent the same course as the measured data but they are shifted to lower values for the cold passage and larger values for the warm passage. This means that the heat transfer rate in the simulation is smaller than given by the experiments in agreement with the too small heat transfer coefficient estimated by the standard correlations (see Section 3.1). Again we assume that the reasons for the deviations are found in the penetration of joining material into the channels causing a differing heat transfer behavior compared to the ideal channel geometry. In addition heat transfer takes place outside the heat exchanger core, especially in the ceramic tubes. Applying TwoPorFlow to a compact metallic crossflow heat exchanger composed of 1700 microchannels with the size of 0.1 mm × 0.2 mm such deviations did not appear [9]. Due to the smaller size of the channels and a much larger heat transfer area density (10,000 m^{-1}) the heat exchanger core dominates pressure loss and heat transfer compared to external effects of media supply. The problem of partial channel blocking does not exist using metallic structure components joined by diffusion welding.

4. Conclusions

Counterflow and crossflow micro heat exchangers made of alumina were fabricated and successfully tested with water flow rates of up to 120 kg/h. The efficiency was in the range of 0.10–0.22. Heat transfer coefficients for the crossflow heat exchanger of up to 22 kW/m^2 K were reached. The experimental results like pressure loss and heat transfer were compared to estimations by standard heat exchanger correlations and more detailed numerical simulations using a porous body approach. It became evident that the geometry of the fluid channels is influenced by the joining process of the ceramic components changing the characteristics of pressure loss and heat transfer which is nearly impossible to realize in simulations. The present micro heat exchangers made of ceramic are composed of a small number of structured plates with a small exchange surface area density compared to metallic compact microchannel heat exchangers leading to a stronger influence of processes in the supplying pipes which cannot be fully described in a porous body approach.

References

[1] P.M. Martin, D.W. Matson, W.D. Bennett, D.C. Stewart, C.C. Bonham, IMRET 4, Topical Conference Proceedings, AIChE Spring National Meeting, Atlanta, GA, USA, March 5–9, 2000, pp. 410–415.
[2] R. Knitter, M. Liauw, Lab Chip 4 (2004) 378–383.
[3] F. Meschke, G. Riebler, V. Hessel, J. Schürer, T. Baier, Chem. Eng. Technol. 28 (2005) 465–473.
[4] K. Schubert, J. Brandner, M. Fichtner, G. Linder, U. Schygulla, A. Wenka, Microscale Therm. Eng. 5 (2001) 17–39.
[5] R. Knitter, D. Göhring, P. Risthaus, J. Haußelt, Microsyst. Technol. 7 (2001) 85–90.
[6] B. Alm, R. Knitter, J. Haußelt, Chem. Eng. Technol. 28 (2005) 1554–1560.
[7] T. Stief, O.-U. Langer, K. Schubert, Chem. Eng. Technol. 21 (1999) 297–303.
[8] Verein Deutscher Ingenieure, VDI-Gesellschaft Verfahrenstechnik und Chemieingenieurwesen (Hsgb.), vol.9, VDI-Wärmeatlas, Berechnungsblätter für den Wärmeübergang, Springer-Verlag, 2002.
[9] U. Imke, Chem. Eng. J. 101 (2004) 295–302.